NANO LETTERS

2006
Vol. 6, No. 3
449−452

Direct Observation of Single-Walled Carbon Nanotube Growth at the Atomistic Scale

Ming Lin,[†] Joyce Pei Ying Tan,[†] Chris Boothroyd,[†] Kian Ping Loh,[‡] Eng Soon Tok,*[,§] and Yong-Lim Foo*[,†]

Institute of Materials Research and Engineering, 3 Research Link, Singapore 117602, Department of Chemistry, National University of Singapore, 3 Science Drive 3, Singapore 117543, and Department of Physics, National University of Singapore, 2 Science Drive 3, Singapore 117542

Received November 30, 2005; Revised Manuscript Received January 23, 2006

ABSTRACT

The growth dynamics of a single-walled carbon nanotube (SWNT) is observed in *real-time* using an in situ ultrahigh vacuum transmission electron microscope at 650 °C. SWNTs preferentially grow on smaller sized catalyst particles (diameter ≤ 6 nm) with three distinct growth regimes (incubation, growth, and passivation). All of the observed SWNTs grow via a base-growth mechanism with C diffusion on active Ni catalyst sites. Under the same experimental conditions, formation of carbon nanocages was observed on larger Ni catalyst particles. The evolution of SWNTs or nanocages is dependent on catalyst size, and this can be rationalized from both energetics and kinetics considerations.

Controlled fabrication of nanostructured materials is a crucial step underlying all fields of nanotechnology. This requires a detailed understanding of the growth mechanism and identifying the salient processing parameters for selective growth of these nanoscale structures. In the case of carbon-based nanostructures, comprehending growth pathways is therefore the basis for large-scale industrial production of high-quality carbon nanotubes (CNTs) with controlled helicity, length, and diameter for technological applications.[1]

Carbon-based nanostructures can be grown by arc discharge, laser ablation, and chemical vapor deposition (CVD). Among them, CVD is the most attractive candidate for industrial adoption because of its scalability and low cost. Most CNT formation mechanisms have been studied by theoretical calculations[2,3] or postdeposition high-resolution transmission electron microscopy (TEM).[4−11] Often, CVD growth using the same experimental growth condition yields "different" types of structures (e.g., SWNTs, double-walled nanotubes (DWNTs), multiwalled nanotubes (MWNTs), and amorphous tubes),[12−16] making complete and detailed understanding of reactions difficult. This is further aggravated by the ambient/low vacuum growth conditions that convolute data with contaminants. The mechanism of carbon nanostructure growth by CVD is marred by long-standing disagreement. Baker and co-workers[17,18] proposed that hydrocarbon gases undergo catalytic decomposition on the surface of metal particles to form carbon adsorbates, which, driven by the concentration gradient, diffuse through the bulk of the metal before precipitating in the form of graphene on different surface sites of the catalyst. De Bokx et al.[19] contradict this hypothesis and proposed that the catalyst is converted to intermediate metal carbides during growth before decomposing to graphene layers. There is, however, no validation of either mechanism because of the absence of experimental proof of the structure of the catalyst during *steady-state* growth at elevated temperature in a controlled environment. Most previous studies by TEM were carried out after growth, in ambient conditions, where the structure of the catalyst could have undergone transition to a phase entirely different from steady state at growth.[8]

In situ ultrahigh vacuum (UHV) TEM, operating in both direct and reciprocal space, is an ideal platform for conducting these experiments because of its capability for real time observation on the nanometer scale. This enables quantitative investigation of the reaction pathways and growth kinetics of carbon nanostructures at elevated temperatures.[20−22] In this letter, we report in situ UHVTEM (base pressure $\sim 1 \times 10^{-9}$ Torr) experimental results of SWNT growth using a Ni−MgO catalyst by the catalytic decomposition of acetylene (C_2H_2). We expound the influence of catalyst size on the formation of different carbon nanostructures. In addition, we also identify the steady-state catalyst structure and for the

* Corresponding authors. E-mail: phytokes@nus.edu.sg; yl-foo@imre.a-star.edu.sg.
[†] Institute of Materials Research and Engineering.
[‡] Department of Chemistry, National University of Singapore.
[§] Department of Physics, National University of Singapore.

10.1021/nl052356k CCC: $33.50
Published on Web 02/15/2006

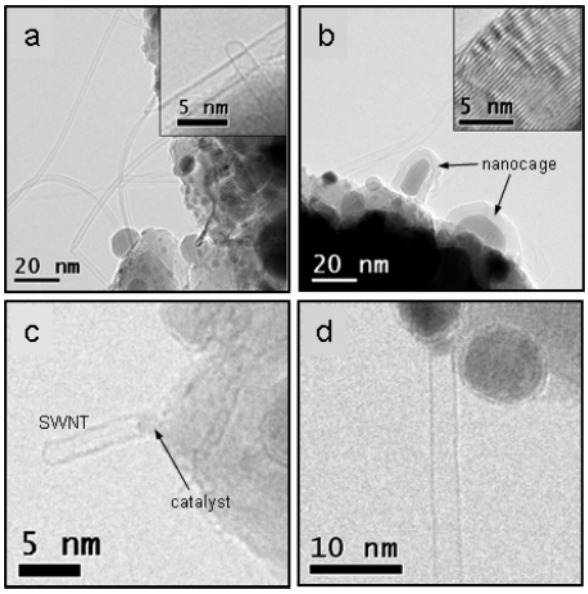

Figure 1. TEM images acquired after growth. (a) Bundled SWNTs; (b) nanocages; (c and d) base growth of SWNTs showing a direct relationship between Ni catalysts and diameters of SWNTs.

first time, resolve through direct experimental data, the CNT's growth mechanism.

Ni−MgO[13] precursors were prepared by coprecipitation from a mixture of $Ni(NO_3)_2$ and $Mg(NO_3)_2$ solutions at a molar ratio of 1:1. The precipitates obtained were dried at 100 °C, ground into powders, calcined in air at 700 °C for 2 h to decompose the nitrites, and then reduced in a H_2 atmosphere at 700 °C for 2 h to form reactive Ni nanoparticles on an MgO substrate. The Ni−MgO catalysts were ultrasonically dispersed in absolute ethanol and then cast on a holey carbon-coated Mo grid that was then mounted over a Si heater. C_2H_2 was passed into the TEM column through a leak valve. The microscope had a backfilled pressure of $\sim 4 \times 10^{-6}$ Torr during the reaction, and the temperature of the catalyst was maintained at 650 °C. Growth of SWNTs and carbon nanostrutures was captured using both Gatan DV300 and GIF2000 image acquisition systems.

Our catalyst preparation technique through wet chemistry yields Ni with a high dispersity in diameter. This enables us to study the effect of catalyst dimension within *a single experiment*, with all other experimental conditions *remaining constant* in the in situ TEM. We can, therefore, make a direct inference of the effect of size and morphology of the catalyst on the type of carbon nanostructure grown. During growth at $T = 650$ °C and $P_{C_2H_2} = 4 \times 10^{-6}$ Torr, we observed the formation of SWNTs and nanocages. Figure 1a and b shows typical TEM images of the SWNTs and nanocages produced after cooling the products. The SWNTs have diameters ranging from about 0.6 to 3.5 nm, with lengths ranging from a few nanometers up to micrometers. The clean surfaces of the SWNTs were free of any amorphous carbon coating. Our TEM images show that all of the SWNT tips are closed and there are no catalyst particles at the tips, indicating that all of the SWNTs follow the base-growth mechanism. Under our experimental conditions, the smaller Ni catalyst particles (diameter < 6 nm) favor formation of SWNTs, whereas

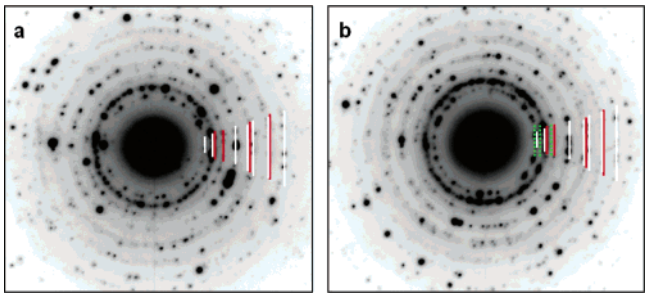

Figure 2. Diffraction pattern of Ni−MgO catalysts (a) before and (b) during reaction. White and red lines indicate diffraction from crystalline MgO and Ni particles, respectively. Green dotted lines indicate the expected diffraction ring position for Ni_3C crystals.

larger catalyst particles favor nanocage formation. There appears to be a size selection of catalyst in determining the type of final products. The active spherical Ni particles for the growth of SWNTs are mainly nonfaceted particles. A close examination of the base of the nanotubes using magnified TEM images reveals that the ratio of the Ni particle diameter to the nanotube diameter lies between 0.5 and 1, indicating that the diameter of nanotubes is correlated to the size of the Ni nanoparticles supported on MgO, as indicated in Figure 1c and d. This insight developed through the in situ TEM experiment suggests that we can grow SWNTs with *controlled diameters* for technological application through engineering nanoscale catalyst dimensions.[5,6,23]

To resolve the disagreement on reaction pathways as proposed by Baker et al.[17,18] and De Bokx et al,[19] we used selected area electron diffraction patterns (DP) to follow the crystal structure of the catalyst both before and during growth at 650 °C. Figure 2a is the DP of the Ni−MgO catalyst before C_2H_2 exposure, and Figure 2b is the DP of Ni−MgO during steady-state growth. Both DPs comprise Ni and MgO diffraction rings, indicating that the catalyst particles remain as metallic Ni during growth. We do not observe formation of new diffraction rings corresponding to different *d* spacing during growth. The absence of the intermediate phase Ni_3C in the DPs strongly suggests that the De Dokx et. al. model, where carbides are formed prior to precipitation as carbon nanostructures, is not the operative mechanism during growth of SWNTs and nanocages. Thus, the more plausible mechanism for the formation of these structures is through the nucleation and growth by diffusion of carbon adatoms formed through the catalytic decomposition of C_2H_2 on a metallic Ni catalyst. There are two diffusion pathways, that is, bulk diffusion and surface diffusion to the boundary of the growth interface between the Ni catalyst and the CNT (or nanocage) with the latter dominating the reaction pathway by having a lower activation barrier due to a lower coordination number.

First-principle calculations[24] have shown that an extended graphene layer on a Ni catalyst is more stable than an aggregate of isolated carbon atoms on the Ni surface. The difference in free energy therefore provides the driving force for the initial nucleation of carbon adatoms into graphene layers. The growth of these graphene layers resulting in either the formation of a closed-tip SWNT with a hemispherical graphene carbon cap or a graphene sphere−carbon nanocage

suggests that the initial nucleation dynamics of these features depends on the size of the catalyst. The development of a hemispherical graphene cap (precursor to formation of a closed SWNT tip) or a graphene sphere (precursor to formation of nanocage) is driven by the need to minimize the energy associated with nucleation of the graphene layer when constrained to grow and form a nanotube or a nanocage, in particular, the interplay between the surface energy and strain energy per unit volume on a small or large catalyst. A larger catalyst particle possesses lower curvature than that of a smaller catalyst particle, and this allows the formation of a graphene sphere that envelopes the catalyst particle with lower strain energy because the torsional stress on the C−C bond within the graphene sheet is smaller. The torsional stress within the graphene layers will increase with decreasing dimensions of the catalyst particle, and the build up in strain energy will dominate the total energy, thus making graphene sphere formation unlikely for small catalyst particles. Instead, a partial ring develops and in this instance a hemispherical graphene cap is formed. The built up strain energy is relaxed by allowing tubular growth with the cap as the tip. This is analogous to the island shape transitions observed in strain layer epitaxy where a symmetric shaped island grows to form a wire.[25] Thus, as more carbon atoms are added, the SWNT wall forms and lengthens. This growth model is likened to the yarmulke mechanism.[7] This strain relaxation effect in SWNT growth is also augmented by the fact that on a smaller catalyst bulk diffusion can become significant (the diffusion length is comparable to the catalyst diameter) and the catalytic activity for decomposition is higher, thus leading to higher apparent local adatom density for growth.

To gain insight into the dynamical growth of SWNTs, we used a sequence of bright field (BF) images to follow the growth process of a single SWNT. Figure 3a is a BF image of the Ni catalyst at $t = 0$ s. When the C_2H_2 valve was opened, we observed the growth of an SWNT with a diameter of ~3.3 nm, as shown in Figure 3b−d, on a 4-nm Ni catalyst. The growth of these SWNTs, however, does not occur instantaneously. The absence of kinks on the SWNT and its constant diameter suggest that the SWNT has low defect density. Although the thermal vibration of the unsupported extended segment makes the images slightly unclear at 650 °C, we are still able to measure its length as function of growth time and hence calculate its instantaneous growth rate. Figure 4 is a plot of both the length and instantaneous growth rate versus reaction time. The growth of the SWNT appears to occur in three distinctive regimes under the present growth conditions.

Regime I is the initial slow growth regime marked by no discernible elongation of carbon nanotubes. This period lasted for ~50 s, and the interpolated length of the SWNT at $t =$ 50 s is <1 nm. This is followed immediately by regime II where a very rapid increase in growth rate occurs and the SWNT elongates. The growth rate increases from $R_{SWNT} =$ 0.011 nm/s at $t = 50$ s to a maximum value of $R_{SWNT(max)} =$ 0.31 nm/s at $t = 173$ s. The presence of regime I suggests the existence of an incubation period prior to rapid growth

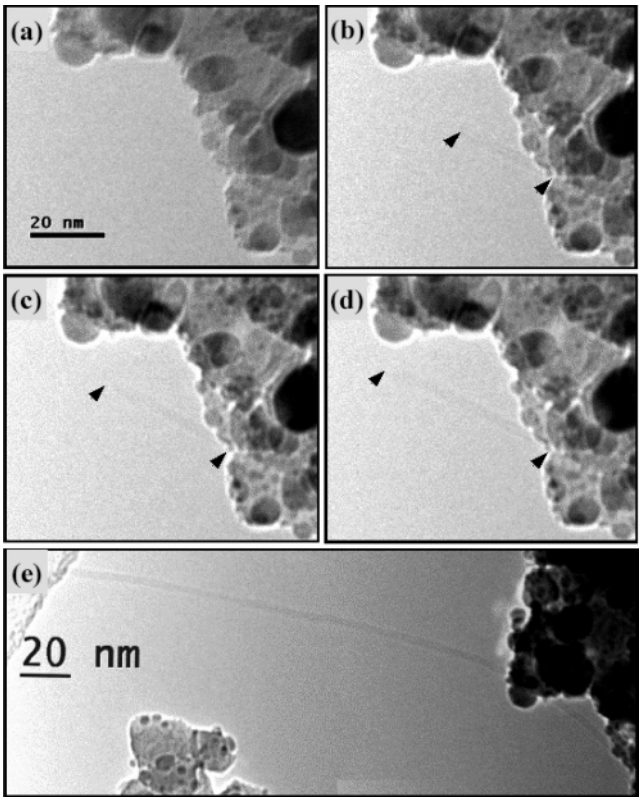

Figure 3. Sequence images of a growing SWNT at (a) 0 s, (b) 96 s, (c) 120 s, and (d) 150 s, with arrows indicating the ends of the nanotube; (e) overview of the whole tube after 1440 s.

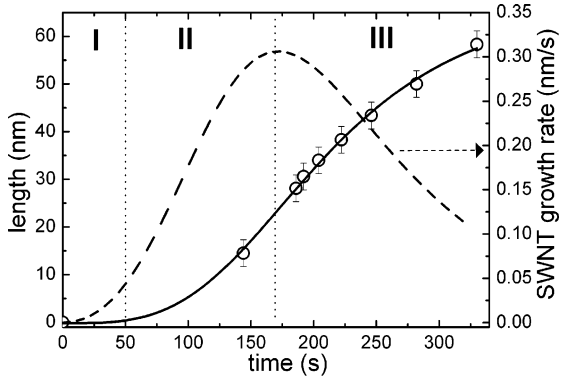

Figure 4. Growth rate and length of a single SWNT as shown in Figure 3.

of SWNTs. Drawing analogy to the incubation period needed for critical nuclei to occur in crystal growth, the initial formation of the graphene layer from diffusing carbon adatoms (i.e., the development a hemispherical graphene cap precursor to the formation of a closed SWNT tip) is thus the slow step in the growth of the SWNT. Assuming an attempt frequency of 10^{13} s^{-1}, the estimated nucleation barrier for carbon adatoms to form the hemispherical graphene cap at 650 °C is ~2.7 eV. The increase in growth rate thereafter is due to incorporation/attachment to the SWNT-nucleus/catalyst growth front by diffusion of carbon adatoms formed through the catalytic decomposition of C_2H_2 on the metallic Ni catalyst. At the maximum growth rate of 0.31 nm/s, ~250 carbon atoms were incorporated into the SWNT per second.

In regime III (t > 173 s), a decay in the growth rate of SWNT occurs. Because all experimental parameters (temperature, $P_{C_2H_2}$) remained constant, the reduction in the growth rate in this regime can be attributed to a poisoning effect arising from the presence of strongly adsorbed carbon atoms on the surface of the catalyst. These carbon atoms passivate the active sites and reduce the catalyst's efficiency. In the absence of regeneration, the coverage of active sites will inevitably decrease with time and thereby result in a decrease in the growth rate of the SWNT as observed in Figure 4. The SWNT growth rate is therefore dependent on the number of active sites and in turn will also be dependent on the adsorption rate of C_2H_2. The growth rate can thus be expressed as $R_{SWNT} = k\,[P_{C_2H_2}]^m\,[\theta]^n$, where k is the rate constant, $P_{C_2H_2}$ is the pressure of C_2H_2, θ is the surface coverage of the active surface sites on the Ni catalyst, and m and n are the respective order of the reaction.

In summary, using our growth conditions we observed the growth dynamics of an individual SWNT using in situ UHVTEM and provide the first direct evidence that the catalyst particles remain as metallic Ni, instead of forming the intermediate Ni_3C phase during growth. These SWNTs grow primarily through the base-growth mechanism, and they preferentially grow on smaller sized catalyst particles (diameter ≤ 6 nm). The ratio of the SWNT to catalyst diameters is ∼0.5−1. Under the same experimental conditions, larger Ni catalyst particles (diameter > 6 nm) result in the formation of nanocages. The size of the catalyst particle has a strong influence on the final grown structure (SWNT or nanocages), and this can be understood from energetics and kinetics considerations. The growth mechanism proposed, based on our experimental observations, is likely to be dependent on experimental conditions and also on the catalyst type. Hence, it will be of great interest to map the formation of carbon nanostructures in terms of the type, size, and growth rates as a function of the growth temperature, catalyst type (Co or Fe), reaction gas, and pressure.

References

(1) Dresselhaus, M. S.; Dresselhaus, G.; Eklund, P. C. *Science of Fullerences and Carbon Nanotubes*; Academic: San Diego, 1996.
(2) Brabec, C. J.; Maiti, A.; Roland, C.; Bernholc, J. *Chem. Phys. Lett.* **1995**, *236*, 150−155.
(3) Deng, W.; Xu, X.; Goddard, W. A. *Nano Lett.* **2004**, *12*, 2331.
(4) Bower, C.; Zhou, O.; Zhu, W.; Werder, D. J.; Jin, S. *Appl. Phys. Lett.* **2000**, *77*, 2767.
(5) Zhang, Y.; Li, Y.; Kim, W.; Wang, D.; Dai, H. *Appl. Phys. A* **2002**, *74*, 325.
(6) Li, Y.; Liu, J.; Wang, Y. Q.; Wang, Z. L. *Chem. Mater.* **2001**, *13*, 1008.
(7) Nikolaev, P.; Bronikowski, M. J.; Bradley, R. K.; Rohmund, F.; Colbert, D. T.; Smith, K. A.; Smalley, R. E. *Chem. Phys. Lett.* **1999**, *313*, 91.
(8) Cui, H.; Yang, X.; Simpson, M. L.; Lowndes, D. H.; Varela, M. *Appl. Phys. Lett.* **2004**, *84*, 4077.
(9) Anderson, P. E.; Rodriguez, N. M. *Chem. Mater.* **2000**, *12*, 823.
(10) Hafner, J. H.; Bronikowski, M. J.; Azamian, B. R.; Nikolaev, P.; Rinzler, A. G.; Colbert, D. T.; Smith, K. A.; Smalley, R. E. *Chem. Phys. Lett.* **1998**, *296*, 195−202.
(11) Little, R. B. *J. Cluster Sci.* **2003**, *14*, 135−185.
(12) Dresselhaus, M. S.; Dresselhaus, G.; Avouris, P. H. *Carbon Nanotubes*; Springer: Berlin, 2001.
(13) Liu, B.; Zhong, Z.; Ding, J.; Lin, J.; Shi, Y.; Si, L. *J. Mater. Chem.* **2001**, *11*, 2523.
(14) Loh, K. P.; Lin, M.; Yeadon, M.; Boothroyd, C.; Hu, Z. *Chem. Phys. Lett.* **2004**, *387*, 40.
(15) Li, Y.; Kim, W.; Zhang, Y.; Rolandi, M.; Wang, D.; Dai, H. *J. Phys. Chem. B* **2001**, *105*, 11424.
(16) (a) Kong, J.; Cassell, A. M.; Dai, H. *Chem. Phys. Lett.* **1998**, *292*, 567. (b) Kong, J.; Soh, H.; Cassell, A. M.; Quate, C. F.; Dai, H. *Nature* **1998**, *395*, 878.
(17) Jong, K. P.; Geus, J. W. *Catal. Rev. Sci. Eng.* **2000**, *42*, 481.
(18) De Bokx, P. K.; Kock, A. J. H. M.; Boellaard, E.; Klop, W.; Geus, J. W. *J. Catal.* **1985**, *96*, 454.
(19) Yasuda, A.; Kawase, N.; Mizutani, W. *J. Phys. Chem. B* **2002**, *106*, 13294.
(20) Yasuda, A.; Kawase, N.; Banhart, F.; Mizutani, W.; Shimizu, T.; Tokumoto, H. *J. Phys. Chem. B* **2002**, *106*, 1849.
(21) Helveg, S., et al. *Nature* **2004**, *427*, 426.
(22) Cheung, C. L.; Kurtz, A.; Park, H.; Lieber, C. M. *J. Phys. Chem. B* **2002**, *106*, 2429.
(23) Lee, Y. H.; Kim, S. G.; Tománek, D. *Phys. Rev. Lett.* **1997**, *78*, 2393.
(24) Tersoff, J.; Tromp, R. M. *Phys. Rev. Lett.* **1993**, *70*, 2782.
(25) Hata, K., et al. *Science* **2004**, *306*, 1362.

NL052356K